Investigation of solar assisted air source heat pump heating system integrating compound parabolic concentrator-capillary tube solar collectors

Li Wei Yang[a], Rong Ji Xu[b], Wen Bin Zhou[c], Yan Li[d], Tong Yang[e], Hua Sheng Wang[a*]

[a]School of Engineering and Materials Science, Queen Mary University of London, Mile End Road, London E1 4NS, UK
[b]Beijing University of Civil Engineering and Architecture, Beijing 100044, China
[c]Department of Mechanical Engineering, Imperial College London, London SW7 2AZ, UK
[d]Geological Institute, China University of Geosciences, Wuhan, Hubei 430074, China
[e]Faculty of Science and Technology, Middlesex University, London NW4 4BT, UK

Abstract

Solar assisted air source heat pump heating systems are capable of achieving green heating where solar availability essentially affects its operation performance and application potentials, especially in higher-latitude regions, such as UK. Compound parabolic concentrator solar collectors can achieve high collector efficiency at high hot water temperature, benefitting to improve solar collection and corresponding thermal energy storage capacities. Though compound parabolic concentrator solar collectors have been widely investigated, application of such collector for solar assisted air source heat pump system is not studied yet. The paper reports numerical simulations of solar assisted air source heat pump heating systems that integrate compound parabolic concentrator-capillary tube solar collectors for domestic heating in the UK. The results show that, for the same seasonal performance factor, the size of the concentrated solar collector required is 12 m^2 whereas the size of the flat plate solar collector required is 18 m^2. This suggests one third reduction in the size of solar collector, significant reduction in cost and convenience for installation. The results also show the potential to further reduce the size of the concentrated solar collector to 9 m^2 or less. The high collector efficiency of the compound parabolic concentrator-capillary tube solar collector enables much small size of solar collector, significantly lower cost and convenient for installation and wide rollout of solar assisted air source heat pump heating system to locations where solar irradiance is relatively lower.

Highlights

* Corresponding to: H.S. Wang, School of Engineering and Materials Science, Queen Mary University of London, Mile End Road, London E1 4NS, UK
E-mail: h.s.wang@qmul.ac.uk

• Integration of concentrated solar collectors with heat pump heating system has been studied.

• Concentrator solar collector leads to potentially 50% size reduction.

• Using concentrated solar collector obtains yearly seasonal performance factor of 4.7.

• Concentrated solar collector enables application of the system to low solar irradiance.

Keywords: Compound parabolic concentrator-capillary tube solar collector, Solar assisted air source heat pump, Domestic heating, Numerical simulation

1. Introduction

Solar assisted air source heat pump (SAASHP) heating systems are a promising technology to achieve a clean future. Solar availability plays an important role on its operation performance and application potentials, especially in higher-latitude regions, such as UK. To improve system performance, improvements on solar collector specifically for SAASHP is an important approach [1]. Currently, flat plate collector (FPC) is commonly used for SAASHP [2]. Some studies attempted to use evacuated tube collector (ETC) as an alternative. Liang et al. [3] established a model for SAASHP using ETC and verified by experiments. Simulation results suggests that, as collector area increases from 10 to 30 m^2, the maximum coefficient of performance (*COP*) increases from 4.3 to 5.0. Huan et al. [4] simulated two types of SAASHPs for university bathroom with an ETC of 860 m^2. The serial heating system achieved a *COP* of 4.87 and the parallel heating system even obtained a *COP* of 10-20 under the weather conditions in Xi'an, China. Vega and Cuevas [5] compared the performances of SAASHP using ETC and uncovered FPC. For space heating (SH), the system using ETC can achieve seasonal performance factor (*SPF*) of 3.8-4.7 while the system using FPC obtained an *SPF* of 3.7-3.8; for hot water (HW), the system using ETC had an *SPF* of 3.3-4 while the system using FPC had an *SPF* of 2.8-2.9. Liu et al. [6] simulated a SAASHP heating system using ETC in alpine regions, which achieved a *COP* of 2.3-4.2 for a collector area of 10 m^2. Caglar and Yamali [7] designed a SAASHP using ETC that obtained a *COP* of 5.56. Wang et al. [8] established a SAASHP for SH, HW and space cooling (SC) using ETC. In SH mode, the *COP* can be 3.75-4.72. Shan et al. [9] adopted ETC in an SAASHP system which achieved *COP* from 2.5 to 3.0.

Some researchers designed solar collectors to match the requirements for SAASHP. Kuang et al. [10] modified a steel radiator with a structure of dimpled and spot-welded plates as collector. This system realised a *COP* of 2.19. He et al. [11] experimentally studied a

SAASHP heating system using heat pipe as the solar collector and reached a *COP* of 4.93 for a collector area of 2.4 m^2. Buker and Riffat [12] designed a solar roof that integrated the solar collector with the building structure. With a solar roof area of 1.92 m^2, the *COP* of the system was 2.29. Lee et al. [13] designed an air-based flexible solar collector. It has reflective film to reflect solar irradiance with low incident angle to the absorbing tube. Using this collector, the SAASHP achieved a *COP* of 1.12-3.99. Kim et al. [14] adopted collector/evaporator in SAASHP and achieved a *COP* of 3.4. Treichel and Cruickshank [15] designed an air-type solar collector where air was used as the working fluid and also as the thermal energy storage (TES) medium. Their experimental results showed a *COP* of 1.9-2.4 and simulation results showed a reduction in greenhouse gas by even 37.5 tonnes CO_2 equivalent [16].

Although different designs of solar collectors have been developed to enhance the performance of SAASHP as summarised in table 1, the operation of SAASHP is still strongly limited by solar availability. Further studies are needed to promote the utilisation of SAASHP in wide regions. The compound parabolic concentrator (CPC) concentrates the incidence of solar irradiance onto the designed surface areas and has been used to increase the efficiency and outlet water temperature of solar collectors, benefitting to improve solar collection and corresponding thermal energy storage capacities. Different types of CPC solar collectors have been proposed. Gao and Chen [17] proposed a multi-sectional CPC with an average optical efficiency of 96.7%. Chen and Yang [18] investigated an asymmetric CPC-ETC to harvest energy in winter (with an optical efficiency of 0.7) and avoid overheating in summer (with an optical efficiency of 0.39). Zheng et al. [19] designed a CPC-copper tube solar collector which achieved a collector efficiency of 60.5%. Chamasa-Ard et al. [20] designed a CPC-ETC which achieved a collector efficiency of 78.0%. Wang et al. [21] developed a CPC-heat pipe ETC which achieved a collector efficiency of 60.0%. Xu et al. [22] developed a CPC-capillary tube solar collector (CSC) which achieved collector efficiency of 75%. Compared with other CPC solar collectors, the CPC-CSCs can achieve a higher collector efficiency at higher collecting temperatures. Indira et al. [23] designed a dual-concentration collector using CPC, parabolic trough concentrator and dual-axis tracking. With the assistance of CPC, the maximum optical efficiency of this collector is around 6.35% higher than solely using parabolic trough concentrator. However, current studies on the utilisation of CPC collectors in SAASHP for higher latitude regions is rare. Wei et al. [24] economically investigated a SAASHP for space heating of a rural building using heat pipe, FPC, ETC and CPC and recommended heat pipe collectors for utilisation. Chen et al. [25] economically investigated CPC for an absorption heat pump and obtained a *COP* of only 1.04 for heating. The technical details for the operation performance of a SAASHP system using CPC collectors are needed to reveal the effect of CPC collectors on the promotion of SAASHP in regions with lower solar availability.

The present work incorporates the CPC-CSC with the SAASHP heating system and studies the system performance in London (51.5 ^{o}N, UK) over a typical metrological year. A module of CPC-CSC is developed and self-coded in TRNSYS 17 based on data from the numerical model developed and verified in [22]. Thus, the numerical model for the SAASHP heating system using CPC-CSC is established. The heating system operates to provide space heating (SH) and hot water for a single-family house (SFH) 45 building [26]. The operation performance of the system is then compared with the system using FPC in [27]. The effects of collector area on the system performance (such as electricity consumption, *COP* and *SPF*) are analysed for collector areas of 6 m^2, 9 m^2, 12 m^2, 15 m^2 and 18 m^2, respectively. Furthermore, economic analysis is conducted for different collector areas considering the current electricity price.

Table 1: SAASHP heating systems integrating different solar collectors

Authors	Location	Function of HP	Refrigerant	Solar collector type	Solar collector area (m^2)	TES (m^3)	T_a (°C)	*HC* (kW)	*COP*	*SPF*
Liang et al., 2011 [3]	-	SH	R22	evacuated tube	10	-	-1.2-9.5	10	3.3-4.3	-
					20				3.3-4.6	-
					30				3.3-5	-
Huan et al., 2019 [4]	Xi'an, China 34 °N	HW	-	evacuated tube	860	55	24-37	2.8×10^6-3.2×10^6	4.87	-
					860			2.7×10^6	10-20	-
Vega and Cuevas, 2020 [5]	-	SH	-	evacuated tube	22.5	0.3	10.2	-	-	3.8-4.7
				uncovered	22.5				-	3.7-3.8
		HW	-	evacuated tube	225	22.7	10.2	-	-	3.3-4
				uncovered	225				-	2.8-2.9
Liu et al., 2020 [6]	Xining, China 36.6 °N	SH	-	evacuated tube	10	0.8	-18.2-29.88	-	2.3-4.2	-
Caglar and Yamali, 2012 [7]	-	SH	R407C	evacuated tube	-	0.12	-	5.87	5.56	-
Wang et al., 2015 [8]	-	SC, SH, HW	R407C	evacuated tube	-	0.15	7, 12, 20	2.56-4.24 (SH)	3.75-4.72 (SH)	-
Shan et al., 2016 [9]	Beijing, China 40°N	SH	-	evacuated tube	-	0.72, 0.8	-13.3-4.5	3.9	2.5-3.0	-
Kuang et al., 2003 [10]	Qingdao, China 36°N	SH, HW	-	coated, covered	11	2.1	-10-4	4.99	2.19	-
He et al., 2015 [11]	London, UK 51°N	HW	R134a	covered, heat pipe	2.4	0.03, 0.2	25	2.253	4.93	-
Buker and Riffat, 2017 [12]	-	SH, HW	R134a	solar thermal roof	1.92	0.055	27	-	2.29	-
Lee et al., 2018 [13]	Seoul Korea, 37 °N	HW	R1233zd(E), R134a	air-based flexible solar collector	35.2	0.6	2.08-10.92	0.83-3.29	1.12-3.99	-
Kim et al., 2018 [14]	-	HW	R134a	collector/evaporator	24	-	21	7.21	3.4	-
Treichel and Cruickshank, 2021 [15], [16]	-	HW	R134a	air-type solar collector	1.26	0.189	-	-	1.9-2.4	-
Wei et al., 2019 [24]	Beijing, China 40°N	SH	-	heat pipe, evacuated tube, FPC, CPC	0-40	0-4.36	-9	10	-	-
Chen et al., 2022 [25]	Nanjing, China 32°N	SC, SH	-	CPC	927-2519	0-6 MWh	3	1797 MWh	2.09 (SH)	-

2. Compound parabolic concentrator-capillary tube solar collector

The CPC-CSC is a non-tracking solar collector consisting of CPCs, capillary tubes, a glass cover, insulation layer and baseplate (see Figure 1(a)) [22]. Each CPC unit has an aperture width of 53 mm, a groove depth of 52.5 mm and a concentration ratio of 4.22. The capillary tubes with an outer diameter of 4 mm and an inner diameter of 2 mm are placed and fixed at the circle for involute of the CPC. To reflect all the solar radiation to the absorber surface, the diameter of the circle for involute of the CPC concentrator is set to be the outer diameter of the capillary tubes. The reflective surface is coated of an aluminium foil layer with a thickness of 0.1 mm and a reflectivity of 0.85. Two copper tubes with an outer diameter of 12 mm and an inner diameter of 10 mm work as the inlet and outlet headers connecting the capillary tubes. The single-layer high-transparent glass cover has a thickness of 4 mm. The four sides and the baseplate of the solar collector are insulated to reduce heat loss. Water is used as the working fluid in the previous experiments.

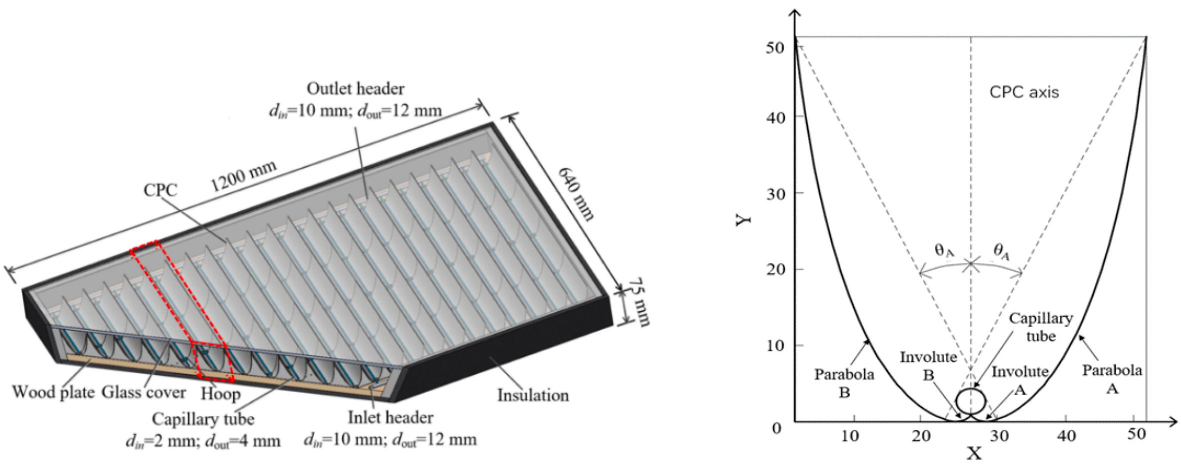

(a) (b)

Figure 1: Structure of CPC-CSC: (a) geometry (b) schematic [22]

The CPC concentrator consists of two pairs of symmetrical curves (circle for involute of the CPC and parabola line) with compound rotation (see Figure 1(b)). The circle for involute of the CPC is defined by Eq. (1) for $0 \le \varphi \le 90° + \theta_A$ [22]:

$$\begin{cases} X = \frac{d}{2}(\sin\varphi - \varphi\cos\varphi) \\ Y = -\frac{d}{2}(\varphi\sin\varphi + \cos\varphi) \end{cases} \tag{1}$$

where φ is the angle between the incident ray and the X-axis. The parabola line is defined by Eq. (2) for $90° + \theta_A \le \varphi \le 270° + \theta_A$:

$$\begin{cases} X = \frac{d}{2}(\sin\varphi - A^* \cos\varphi) \\ Y = -\frac{d}{2}(A^* \sin\varphi + \cos\varphi) \end{cases} \tag{2}$$

where

$$A^* = \frac{\frac{\pi}{2}+\theta_A+\varphi-\cos(\varphi-\theta_A)}{1+\sin(\varphi-\theta_A)} \tag{3}$$

θ_A is the aperture angle of the CPC defined by Eq. (4):

$$\theta_A = \sin^{-1}(\frac{1}{CR}) \tag{4}$$

where *CR* is the concentration ratio, given by Eq. (5):

$$CR = \frac{D}{\pi\times d} \tag{5}$$

where *D* is the aperture width and *d* is the outer diameter of the capillary tube absorber.

2.1 Numerical simulation of heat transfer and verification

Numerical simulations are conducted using Ansys-Fluent for three-dimensional heat transfer of CPC-CSC. One of the CPC units is selected for computation. The geometry of the unit is 600 mm x 53 mm x 75 mm. The parameters specifying the CPC model are listed in table 2 where the working fluid is set to be water.

Table 2: Parameters for the CPC-CSC model [22]

Material	**Thickness (mm)**	**Thermal conductivity (W/m K)**	**Density (kg/m^3)**	**Specific heat (J/kg K)**	Thermal expansion coefficient **(/K)**	**Viscosity (µPa s)**
Glass	4	0.76	2500	790	-	-
Air	-	0.0267	1.225	1005	0.0033	17
Water	-	0.6	998.2	4182	-	1003
CPC material (ABS plastic)	1	0.25	1050	1591	-	-
Thermal insulation material	10	0.034	54	1500	-	-
Capillary tube material (copper)	1	387.6	8978	381	-	-

The solar thermal energy collection in the solar collectors involves conduction, convection, and radiation heat transfer. Convective heat transfer occurs between the outer wall of the capillary tubes and the air layer. The water flow inside the tubes is regarded as a 3D, steady, constant-property, laminar flow. Considering the heat transfer process, governing equations [28] are following:

Conservation of mass:

$$div(U) = 0 \tag{6}$$

Conservation of momentum:

$$div(u\vec{U}) = div(vgradu) - \frac{1}{\rho}\frac{\partial p}{\partial x} \tag{7}$$

$$div(v\vec{U}) = div(vgradv) - \frac{1}{\rho}\frac{\partial p}{\partial y} \tag{8}$$

$$div(w\vec{U}) = div(vgradw) - \frac{1}{\rho}\frac{\partial p}{\partial z} \tag{9}$$

Conservation of energy for heat transfer of air and water flow:

$$div(\vec{U}T) = div(\frac{\lambda}{\rho c_p} gradT) \tag{10}$$

Conservation of energy for heat transfer in solid:

$$\frac{\partial T^2}{\partial x^2} + \frac{\partial T^2}{\partial y^2} + \frac{\partial T^2}{\partial z^2} = 0 \tag{11}$$

For convection of air inside the collector, the Boussinesq assumption is taken to calculate the density.

$$\left(\rho_{\mathrm{a}} - \rho_{\mathrm{amb}}\right) g = -\rho_{\mathrm{amb}}\beta_{\mathrm{a}}\left(T - T_{\mathrm{amb}}\right) g \tag{12}$$

where ρ_a is the air density, ρ_{amb} is the density of ambient air at its temperature T_{amb} and β_a is the thermal expansion coefficient of air.

The boundary conditions for the computational domain are:

Upper and lower surfaces at *x-z* plane y=0, H_{D}: the convection boundary condition with air temperature given;

Front and back end surfaces at *x-y* planes *z*=0, L_{D}: adiabatic condition;

Left and right surfaces at *y-z* planes *x*=0, W_{D}: symmetrical boundary condition.

Air inside collector: The non-slip boundary conditions are applied to all solid-air interfaces.

Water flow in capillary tubes: At the inlet: velocities $u=u_{in}$, $v=0$, $w=0$; temperature $T=T_{in}$; at the outlet: partial unidirectional condition; The non-slip boundary condition is applied to the solid-water interface.

Since the diameter of the copper capillary tubes are small compared with the size of CPCs and hence are regarded as a homogeneous body heat source. All the surface temperatures of solid components are obtained from the coupled numerical simulations of air convection inside the collector, water flowing inside the capillary tubes and heat conduction in the solids.

To verify the model and numerical simulation, a set of experiments were conducted in Beijing, China. The working conditions of the experiments are listed in table 3. The measurements were conducted, and the experimental data were processed according to Chinese standard for the test methods of solar collectors [29]. The experimental results show good agreements with simulation results [22]. Therefore, the simulated results are used to establish the module in TRNSYS.

Table 3: Experimental conditions [22]

	Solar irradiance (W/m^2)	Ambient temperature (K)	Air velocity (m/s)	Date of experiments
Set 1	290-1000	288-291	1-2	10. Oct. 2016-20 Nov. 2016
Set 2	920-1000	289-293	1-2	5 Apr. 2017-10 May 2017

2.2 Empirical formula and module in TRNSYS

The CPC-CSC works to concentrate solar incidence to the outer surface of the capillary tube and converts solar energy into thermal energy, given by Eq. (13):

$$Q_{SC} = IA - Q_{loss,sc} = cm(T_{out} - T_{in}) \tag{13}$$

where I is the global solar irradiance on the tilted surface, A is the collector area, m is the mass flow rate, c is the specific heat of the working fluid, T_{in} and T_{out} are the temperatures of the working fluid at the inlet and outlet of CPC-CSC. $Q_{loss,sc}$ is the heat loss from solar collector to ambient air. Following Dickes et al. [30], the heat loss from the CPC-CSC per meter (along the length direction), Q_{loss}, is calculated by Eq. (14):

$$Q_{loss} = c_0 + c_1(T_{sc} - T_{amb}) + c_2(T_{sc} - T_{amb})^2 + c_3T_{sc}^3 + I(c_4\sqrt{v_a} + c_5T_{sc}^2) + v_a[c_6 + c_7(T_{sc} - T_{amb})] + \sqrt{v_a}[c_8 + c_9(T_{sc} - T_{amb})] \tag{14}$$

where T_{amb} is the temperature of ambient air, v_a is the wind speed. T_{sc} is the surface temperature of CPC-CSC, calculated by Eq. (15):

$$T_{SC} = (T_{in} + T_{out})/2 \tag{15}$$

The weather conditions during the heating season in London are summarised in table 4. According to the standards of system control, the inlet water temperature of CPC-CSC ranges from -5 to 80 °C. Therefore, the parameters given in table 5 are selected for numerical simulation using Fluent. The mass flow rate of water is set at 0.23 kg/h, i.e. 7.23 kg/h-m^2.

Table 4: Weather conditions in London

Parameters	Min	Max	Average
Ambient air temperature, °C	-3.00	18.30	6.61
Solar irradiance on titled surface at 51.5°, W/m^2	0.96	1115.7	199.3
Wind speed, m/s	0.1	14.1	4.23

Table 5: Weather conditions for numerical simulation

Parameters	Values
Solar irradiance on tilted surface, W/m^2	100, 400, 700, 1000
Air velocity, m/s	0, 3, 6, 9, 12, 15, 18, 21, 24
Inlet water temperature of solar collector, °C	0, 25, 50, 75
Ambient air temperature, °C	0, 10, 20

The simulated results are divided into training group (75%) and test group (25%) to train the empirical correlation and avoid overfitting. The correlation obtained from the training group is expressed in Eq. (16):

$$Q_{loss} = 0.1458(T_{sc} - T_{amb}) + 2.3843\times10^{-4}(T_{sc} - T_{amb})^2 - 5.8303\times10^{-6}T_{sc}^3 + I(0.0013\sqrt{v_a} + 8.1302\times10^{-7}T_{sc}^2) + v_a[-0.088 + 5.2377\times10^{-4}(T_{sc} - T_{amb})] + \sqrt{v_a}[0.422 - 0.0104(T_{sc} - T_{amb})] \tag{16}$$

The R^2 of the training group is 0.9903 and that of the test group is 0.9915. This suggests the reliability of the empirical correlation. Based on Eqs. (13) and (16), the CPC-CSC module is established in TRNSYS and is named as Type 219. The flow chart for the operation of CPC-CSC module is shown in Figure 2.

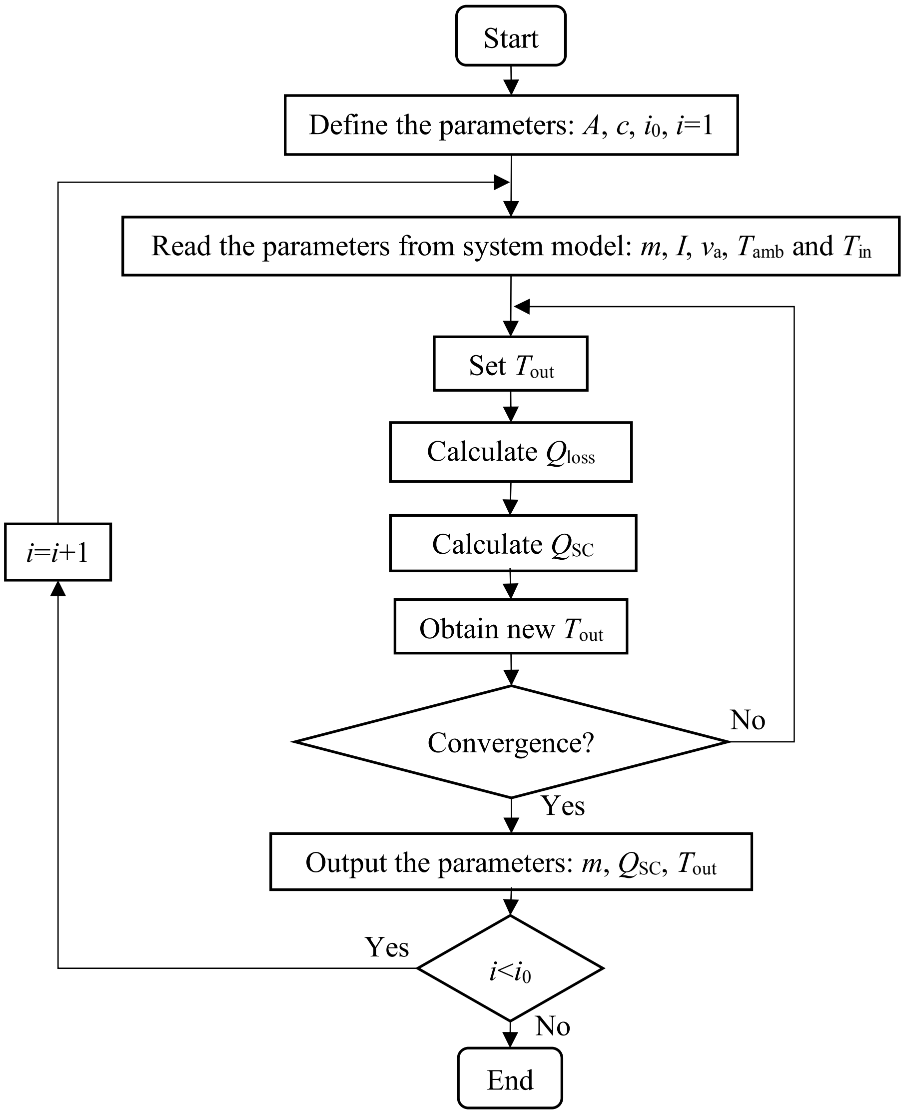

Figure 2: Flow chart for the operation of CPC-CSC module

3. Solar assisted air source heat pump heating system

In this work, a CPC-CSC is applied as solar collector to optimise the operation performance of an indirect expansion SAASHP. The SAASHP includes a solar collector loop, a storage-passive heating loop, a dual-source heat pump unit loop and an end use loop, as shown in Figure 3. In the solar collector loop, the CPC-CSC converts solar energy into thermal energy that is stored in TES tank 1. When TES tank 1 has higher hot water temperature, the TES tank 1 provides thermal energy to TES tank 2. If hot water temperature in TES tank 2 is below 50 ºC, when TES tank 1 has higher water temperature than air temperature, TES tank 1 provides thermal energy to solar-water heat pump (SWHP) and the SWHP works for TES tank 2; or the air source heat pump (ASHP) absorbs thermal energy from ambient air and supplies for TES tank 2. Details about the operation control of the dual-source indirect expansion SAASHP was given in table 6.

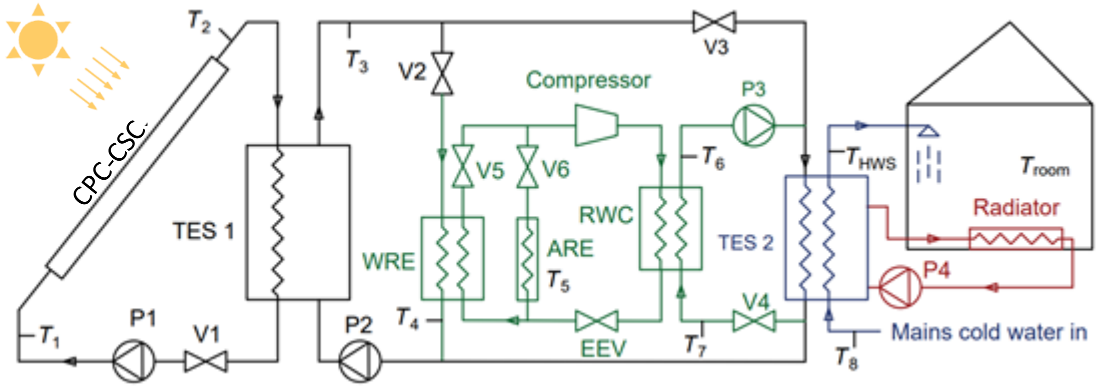

Seven loops in the heating system:

(1) Solar collector loop: SC-TES1-V1-PA-SC

(2) TES1-WRE loop: TES1-V2-WRE-P2-TES1

(3) ASHP loop: ARE-V6-Compressor-RWC-EEV-ARE

(4) space heating loop: TES2-Radiator-P4-TES2

(5) TES1–TES2 loop: TES1-V3-TES2-P2-TES1

(6) RWC-TES2 loop: RWC-P3-TES2-V4-RWC

(7) SWHP loop: WRE-V5-Compressor-RWC-EEV-WRE

SC: Solar collector

TES 1, TES 2: TES tank

V1 - V6: Valve

P1 - P4: Water pump

WRE: Water-to-refrigerant evaporator

ARE: Air-to-refrigerant evaporator

RWC: Refrigerant-to-water condenser

EEV: Expansion valve

T_1 – T_8: Temperature sensor

Figure 3: Schematic of the SAASHP system

Table 6: The rule-based look-up table for control of the dual-source system operation

Operation mode	Temperature range (ºC)	Pumps				Valves						ASHP	SWHP
		P1	P2	P3	P4	V1	V2	V3	V4	V5	V6		
Collector-TES 1	$T_2 > T_3$, $T_{HWS} > 50$	O	X	X	X	O	X	X	X	X	X	X	X
Collector-TES 1-TES 2	$T_2 > T_3 > 50 > T_{HWS}$	O	O	X	X	O	X	O	X	X	X	X	X
Collector-TES 1–SWHP-TES 2	$T_2 > T_3$, $T_{amb} < T_3 < 50$, $T_{HWS} < 50$	O	O	O	X	O	O	X	O	O	X	X	O
ASHP-TES 2	$T_{amb} > T_3$, $T_{HWS} < 50$	X	X	O	X	X	X	X	O	X	O	O	X
TES 1-TES 2	$T_3 > 50 > T_{HWS}$	X	O	X	X	X	X	O	X	X	X	X	X
TES 1–SWHP-TES 2	$T_{amb} < T_3 < 50$, $T_{HWS} < 50$	X	O	O	X	X	O	X	O	O	X	X	O
SH: TES 2	$T_{indoor} < 18$	X	X	X	O	X	X	X	X	X	X	X	X
SH: Collector-TES 1	$T_2 > T_3$, $T_{HWS} > 50$, $T_{indoor} < 18$	O	X	X	O	O	X	X	X	X	X	X	X
SH: Collector-TES 1–TES 2	$T_2 > T_3 > 50 > T_{HWS}$, $T_{indoor} < 18$	O	O	X	O	O	X	O	X	X	X	X	X
SH: Collector-TES 1-SWHP–TES 2	$T_2 > T_3$, $T_{amb} < T_3 < 50$, $T_{HWS} < 50$, $T_{indoor} < 18$	O	O	O	O	O	O	X	O	O	X	X	O
SH: ASHP–TES 2	$T_{amb} > T_3$, $T_{HWS} < 50$, $T_{indoor} < 18$	X	X	O	O	X	X	X	O	X	O	O	X
SH: TES 1-TES 2	$T_3 > 50 > T_{HWS}$, $T_{indoor} < 18$	X	O	X	O	X	X	O	X	X	X	X	X
SH: TES 1–SWHP–TES 2	$T_{amb} < T_3 < 50$, $T_{HWS} < 50$, $T_{indoor} < 18$	X	O	O	O	X	O	X	O	O	X	X	O

Note: Collector: Solar collector. TES 1: Water TES tank1. TES 2: Water TES tank 2.

O: Pumps, SWHP and ASHP are in operation; Valves are open. X: Pumps, SWHP and ASHP are not in operation; Valves are closed.

3.1 Working conditions

The SAASHP system works to provide SH and HW of 300 L/day for a SFH 45 building. The SFH 45 building is modelled according to the parameters in [26]. For weather conditions in London, the space heating periods is determined to be 0-2736 and 7224-8760 hours of the year to ensure indoor air temperature above 15 ^{o}C. The heating season is correspondingly set from 1st October to 30th April. The designed indoor air temperature is 20 ± 2 ^{o}C in the heating season. For reference, at a stable indoor air temperature of 20 ^{o}C, the peak heating load is 3.53 kW and the average heating load is 1.76 kW.

The hot water supply temperature (T_{HWS}) is set to be above 50 ^{o}C to avoid bacteria [31] and below 80 ^{o}C for safety. Hot water temperature at the end use is set at 40 ^{o}C to avoid scalding [32].

3.2 Numerical model in TRNSYS

The numerical simulation is conducted for a typical metrological year, 8760 h, and begins at the middle of the year to observe the continuous heating performance. The simulation time step is set to be 0.017 hour.

The module of CPC-CSC is self-established as mentioned above. For comparison, the collector area of CPC-CSC is set to be the same to that of FPC in [27], 18 m^2. Then the area of CPC-CSC is set to be 6 m^2, 9 m^2, 12 m^2 and 15 m^2 to analyse the influence of solar collector area on the system performance.

To simulate the dual-source heat pump unit, a SWHP module and an ASHP module are used. The parameters of the SWHP module, Type 668, is defined according to the sample file of 30HXC-HP2, Carrier United Technologies and those of the ASHP module, Type 941, is defined based on the sample file of YVAS012, York, Jonson Control. Heating capacities of both modules are set at 8 kW. Details for the module selection and the system connection are shown in Figure 4 and table 7. The parameters that define the models of the components are derived from the experimental data of the component products available in the market.

Table 7: Summary of TRNSYS modules chosen for modelling the components of the heating system and main parameters

Component	Module	Collector area	Parameter	Value
FPC	Type 1b	18 m^2	Inclination angle	51.5^o
			Tested flow rate	30 kg/hm^2
			Intercept efficiency	0.8
			Efficiency slope	13 kJ/hm^2k
			Efficiency curvature	0 kJ/hm^2k^2
CPC-CSC	Type 219 (self-written)	6, 9, 12, 15, 18 m^2	Inclination angle	51.5^o
			Specific heat of working fluid	4.19 kJ/(kg K)
TES tank 1	Type 4a	All	Heat loss coefficient	0.2 W/(m^2 K)
			Volume	500 L
			Height	1.175 m
TES tank 2	Type 4a	All	Heat loss coefficient	0.2 W/(m^2 K)
			Volume	300 L
			height	1 m
ASHP	Type 941	All	Blower power	0.15 kW
			Total air flow rate	1500 l/s
			User defined file	YVAS012, York, Jonson Control
SWHP	Type 668	All	User defined file	30HXC-HP2, Carrier United Technologies

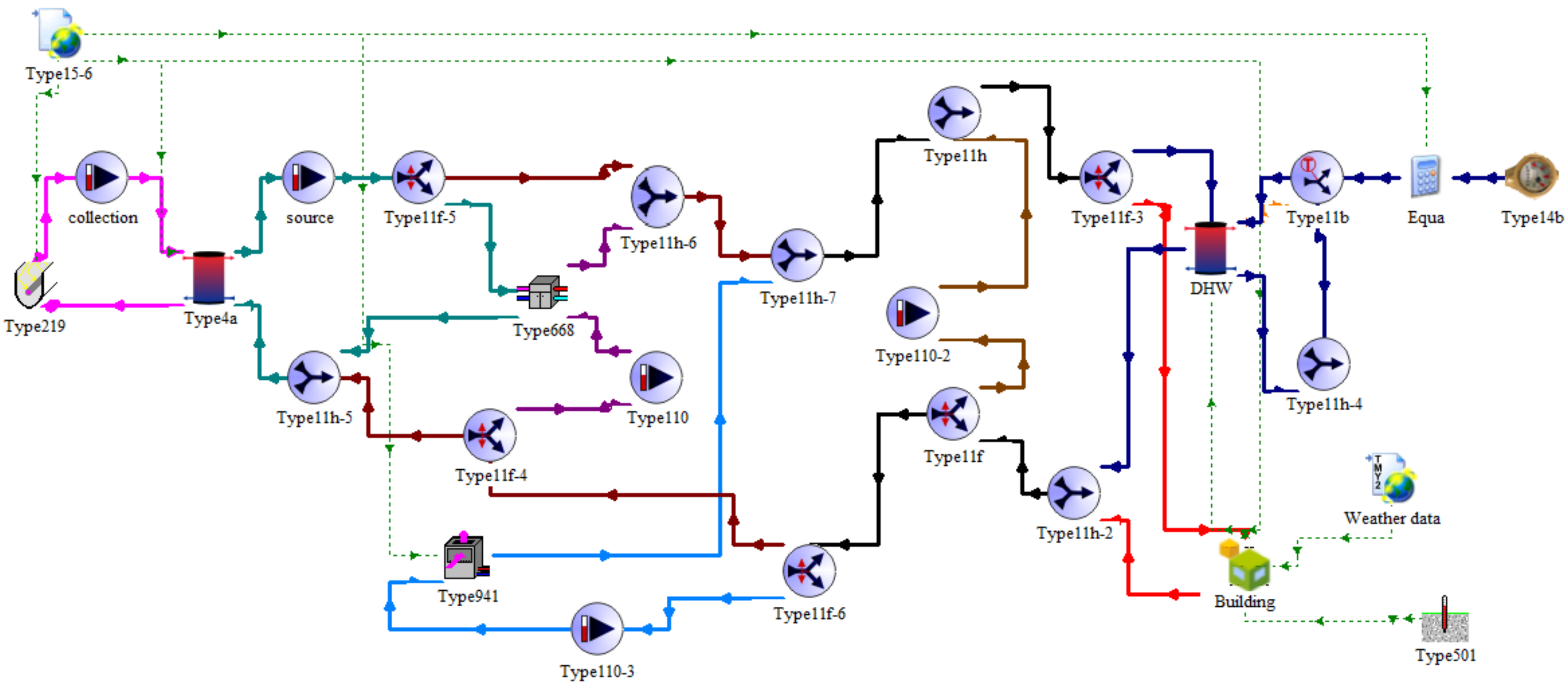

Figure 4: Model of dual-source system using CPC-CSC in TRNSYS

3.3 Performance indicators

The performance of the heating systems is evaluated by a variety of indicators including the room air temperature, HWS temperature, *SPF* of the system (SPF_{sys}), *SPF* of the HP (SPF_{HP}), *COP* of the HP module, and the solar fraction (*SF*). The room air temperature is an indication whether the heat provision by the heating system meets the heat demand of the building. The measured room air temperature is also the quantity that determines the on/off operation of the heating system. The HWS temperature indicates the amount of thermal energy stored in the TES tanks and also determines the on/off operation of the SWHP. The SPF_{sys} describes the overall performance of the whole heating system over the heating season of the year and is defined by Eq. (17):

$$SPF_{sys}=\frac{\int(Q_{SH}+Q_{HW})dt}{\int W_{tot}dt} \tag{17}$$

where Q_{SH} and Q_{HW} are the thermal energies supplied by the system for SH and HW, respectively, and W_{tot} is the total electricity consumed by the HP and all water pumps given by Eq. (18):

$$W_{tot}=W_{HP}+W_{pumps} \tag{18}$$

where W_{HP} is the electricity consumed by the HP calculated by Eq. (19):

$$W_{HP}=j_{ASHP}W_{ASHP}+j_{SWHP}W_{SWHP} \tag{19}$$

where W_{ASHP} and W_{SWHP} are the electricity consumed by the ASHP and SWHP, respectively, j_{ASHP} and j_{SWHP} have values either 1 or 0 representing on or off operation status of ASHP and SWHP. For serial system, $j_{ASHP} = 0$ and $j_{SWHP} = 1$. For parallel system, $j_{ASHP} = 1$ and $j_{SWHP} = 0$. For dual-source system, j_{ASHP} and j_{SWHP} can be 1 or 0, depending on their on/off operation status.

The SPF_{HP} describes the overall performance of a HP over the heating season and is defined by Eq. (20):

$$SPF_{HP}=\frac{\int Q_{HP,con}dt}{\int W_{HP}dt} \tag{20}$$

where $Q_{HP,con}$ is the heat transferred from the condenser of the HP to water circulating to TES tank 2, given by Eq. (21):

$$Q_{HP,\,con}=j_{ASHP}Q_{ASHP,\,con}+j_{SWHP}Q_{SWHP,\,con} \tag{21}$$

where $Q_{ASHP,\,con}$ and $Q_{SWHP,\,con}$ are the heat transferred from the condenser of ASHP and SWHP to water circulating to TES tank 2, respectively.

The *COP* of the HP is defined by Eq. (22):

$$COP=Q_{HP,\,con}/W_{HP} \tag{22}$$

The SF of the heating system, the contribution ratio of the solar thermal energy collected to the system heat provision over the heating season, is defined by Eq. (23):

$$SF = 1 - \frac{\int (Q_{\mathrm{ASHP,con}} + W_{\mathrm{SWHP}})\mathrm{d}t}{\int (Q_{\mathrm{HW}} + Q_{\mathrm{SH}})\mathrm{d}t} \quad (23)$$

4. Results and discussion

Numerical simulations for SAASHP using CPC-CSC have been conducted. The obtained results are compared with those of the SAASHP using FPC to understand the advantages of CPC-CSC. The effects of collector area of CPC-CSC on system performance are analysed.

4.1 Comparison for heating systems using concentrated solar collector and flat plate collector

In this section, performance of system using CPC-CSC of 18 m^2 is compared with that of system using FPC of 18 m^2 [27]. Figure 5 shows the variation of indoor air temperature and hot water supply temperature of systems using different solar collectors in heating season. CPC-CSC can realise high temperature and collector efficiency since the capillary tube reduces the surface area for heat transfer and thus the heat loss from the surface. In addition, horizontal CPC separates the air layer which reduces the convective heat transfer caused by gravity. In non-heating periods, it is more often for system using CPC-CSC to obtain a higher T_{HWS} since CPC-CSC can have a better collection efficiency at higher water temperature. In heating periods, the T_{HWS} of system using CPC-CSC shows less variation than that of system using FPC. This suggests that the high collector efficiency of CPC-CSC benefits for the response speed of the SAASHP to water draw.

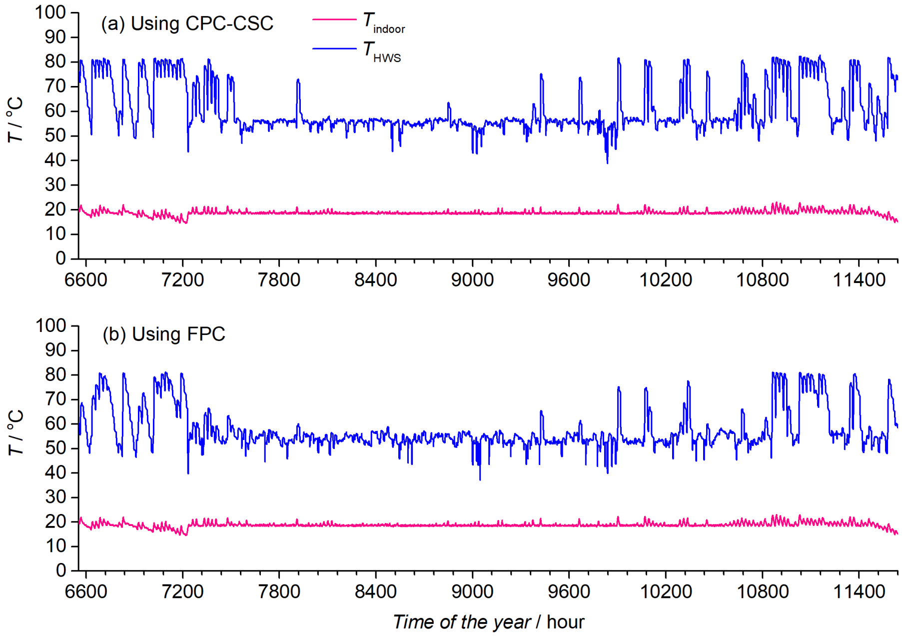

Figure 5: Variations of indoor air temperature and hot water temperature at the outlet of TES tank 2 over a heating season.

Figure 6 shows the heat provision from ASHP, SWHP and direct solar hot water (SHW) over a heating season. The columns are stacked to represent the total daily heat provision. Using CPC-CSC, heat provision by ASHP, SWHP and direct SHW is 6.4 MWh, 1.9 MWh and 1.7 MWh; that for system using FPC is 6.6 MWh, 2.3 MWh, and 1.2 MWh. The results are also summarised in Table 7. Compared with system using FPC, the heat provision from SWHP is significantly reduced by 17.4% using CPC-CSC and the heat provision by ASHP is slightly reduced by 3.0%. Since CPC-CSC can help to obtain higher water storage temperature, more stored hot water in TES tank 1 can be directly used for end use. Using CPC-CSC can apparently increase the heat provision by direct SHW by 41.7%.

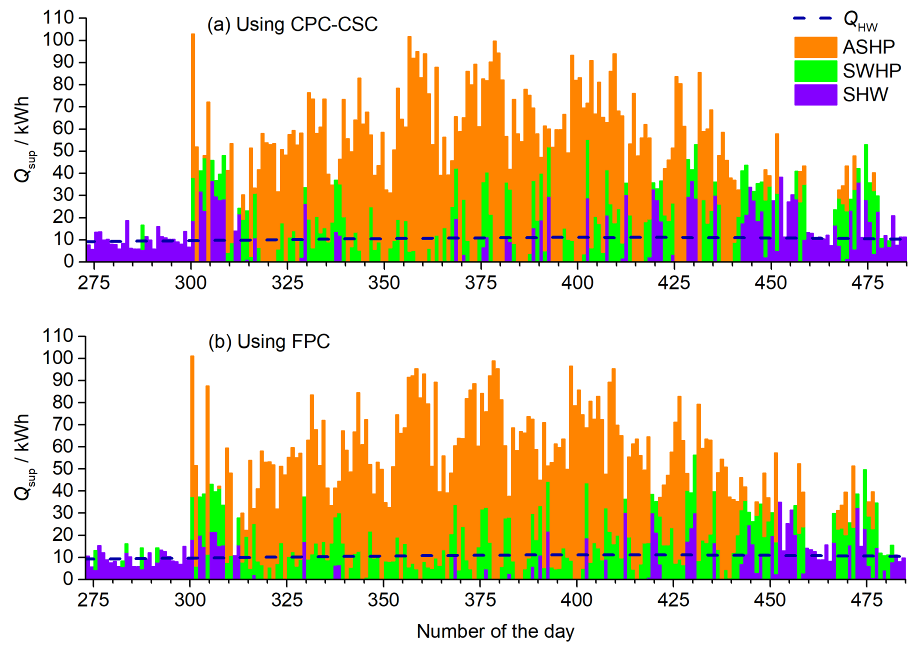

Figure 6: Daily variations of heat for SH and HW by direct SHW, ASHP and SWHP over a heating season

Figure 7 shows the daily electricity consumption of ASHP, SWHP and pumps. The columns are stacked to represent the total daily electricity consumption. The electricity consumptions by ASHP, SWHP and pumps in system using CPC-CSC are 1.69 MWh, 0.37 MWh and 0.28 MWh; those for system using FPC are 1.74 MWh, 0.45 MWh and 0.30 MWh. The results are also summarised in Table 7. Using CPC-CSC can reduce the electricity consumption from all three terms. Since the requirements of pumps to assist SWHP is reduced, though heat provision by SHW is increased, electricity consumption from pumps is reduced in system using CPC-CSC. Overall, compared with the heating system using FPC, the heating system using CPC-CSC can save electricity consumption by 154.5 kWh per year, 123.6 kg CO_2 equivalent.

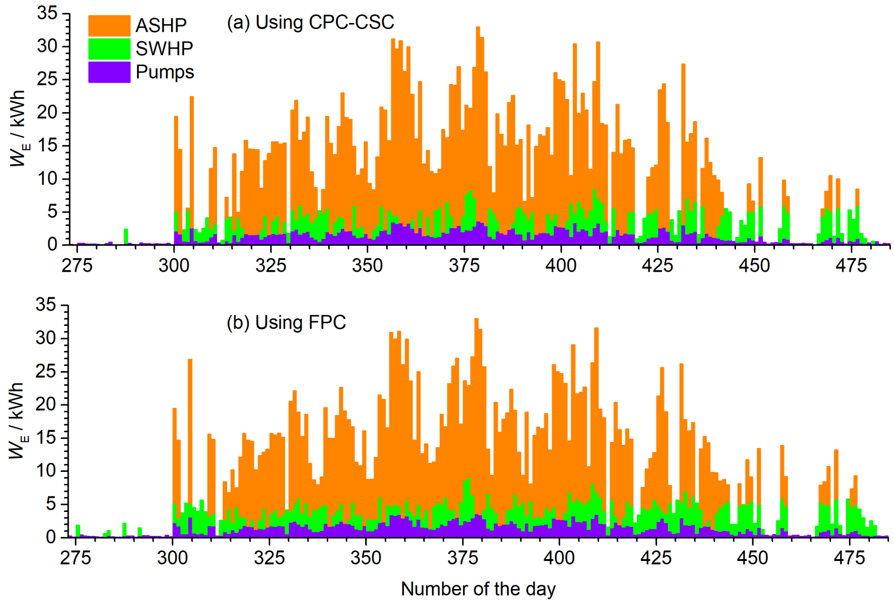

Figure 7: Daily variations of electricity consumption by ASHP, SWHP and pumps over a heating season

Figure 8 shows the daily variation of thermal energy charged (positive) and discharged (negative) in TES tank 2 over a heating season. It can be observed that the heating system using CPC-CSC has larger capacity of Q_{TES} charged in and discharged from TES tank 2. Furthermore, the higher charge and discharge capacities of the TES tank 2 in the system using CPC-CSC reduce the variation frequency of Q_{TES}.

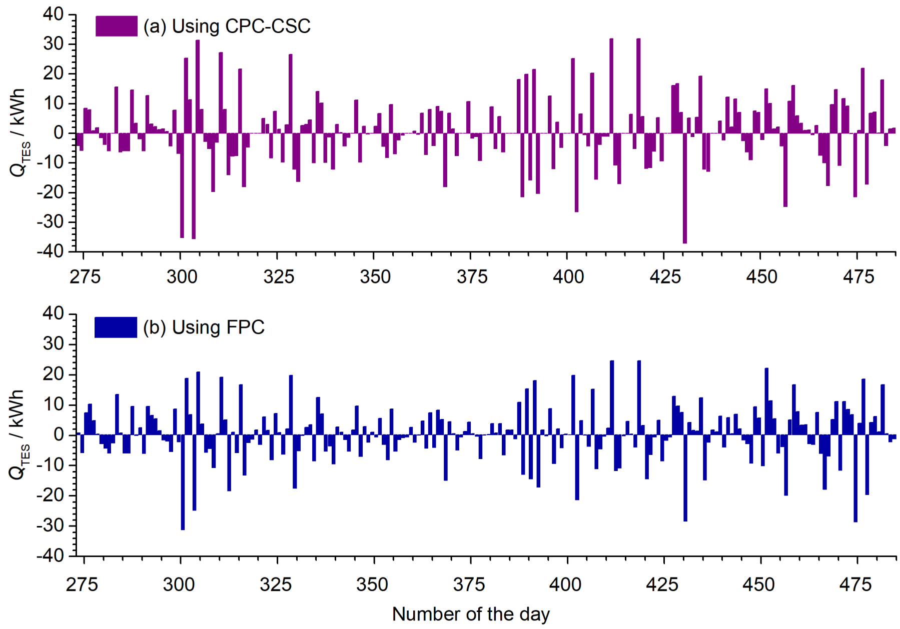

Figure 8: Daily variations of Q_{TES} charged (positive) and discharged (negative) over a heating season

Figure 9 shows the variations of COP_{ASHP} and COP_{SWHP} over a heating season. The average COP_{ASHP} and COP_{SWHP} are 3.5 and 5.1 in system using CPC-CSC and those in system using FPC are 3.5 and 5.0. Using CPC-CSC leads to high water storage temperature in TES tank 1 and thus ASHP only needs to work at higher T_{amb}. However, the system using CPC-CSC are easy to have higher condensing temperature for ASHP and thus average COP_{ASHP} are the same for both systems. At higher water storage temperature in TES tank 1, thermal energy is provided by SHW directly. Operation of SWHP at higher efficiency is avoided in system using CPC-CSC. Thus, for both systems, COP_{SWHP} shows in similar range.

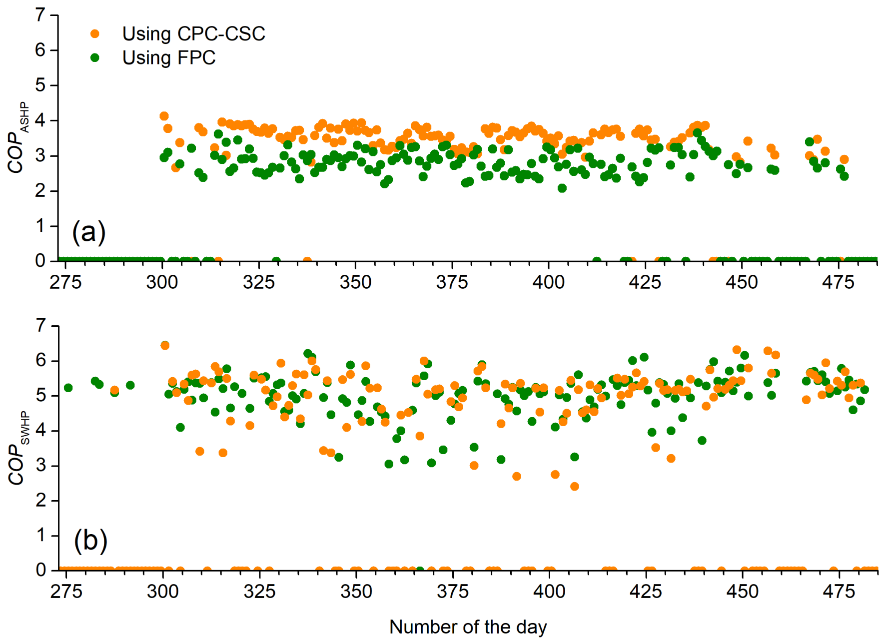

Figure 9: Variations of daily averaged (a) COP_{ASHP} and (b) COP_{SWHP} over a heating season

Figure 10 shows the variations of SPF over a heating season. The SPF_{ASHP} and SPF_{SWHP} are 3.8 and 5.2 in system using CPC-CSC and those in system using FPC are 3.8 and 5.1. In most cases, the heating system using CPC-CSC has higher SPF_{ASHP} and SPF_{SWHP} than the heating system using FPC. Sometimes, the system using CPC-CSC has a lower value, such as on the 316th day (for SPF_{ASHP}) 383rd day (for SPF_{SWHP}). In the case of low SPF_{SWHP} for system using CPC-CSC, water storage temperature in TES tank 1 still meet the operation requirement while that in the system using FPC is low for SWHP operation and ASHP works. Therefore, even though the system using CPC-CSC has a low SPF_{SWHP}, the operation of ASHP are avoided. The overall system efficiency is improved. The heating system using CPC-CSC has a yearly SPF_{sys} of 4.7 while the heating system using FPC has a yearly SPF_{sys} of just 4.4. In heating periods, the SPF_{sys} of the heating system using CPC-CSC is more even than that of the heating system using FPC since system using CPC-CSC relies more on stored solar energy in a stabler range.

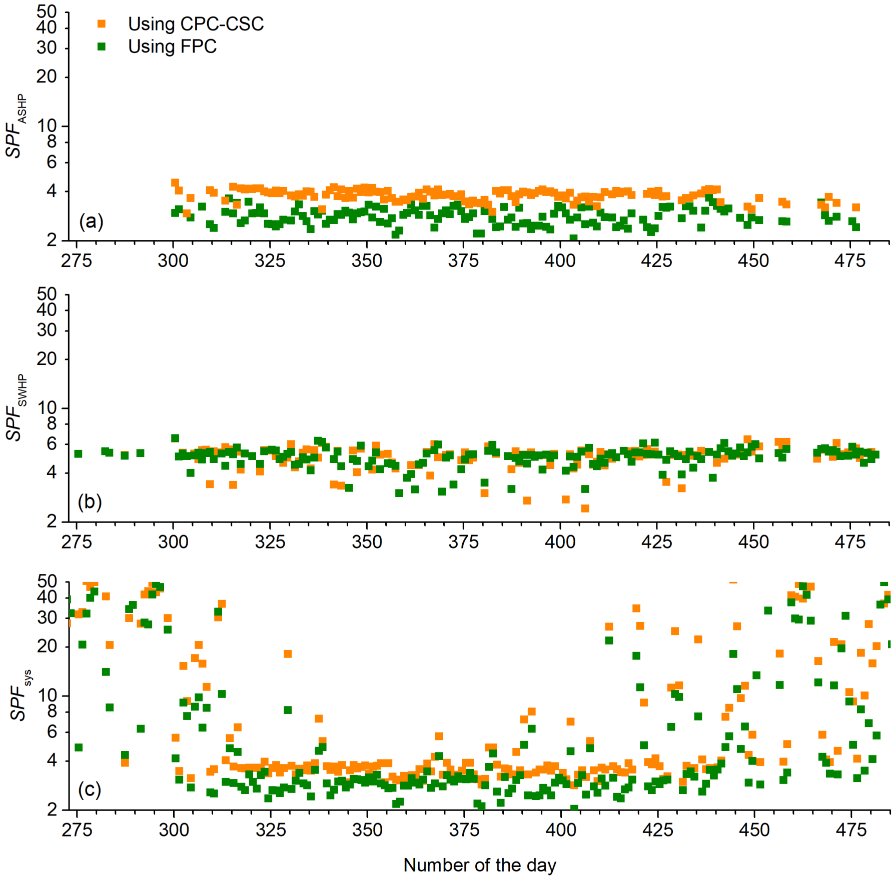

Figure 10: Daily variations of SPF_{ASHP}, SPF_{SWHP} and SPF_{sys} over a heating season

4.2 Effect of area of concentrated solar collector on system performance

The operation performance of the system using CPC-CSC of different areas is compared over a heating season. Figure 11 shows the variations of heat provision from ASHP, SWHP and direct SHW. The columns are stacked to represent the total daily heat provision. The heat provision from ASHP, SWHP and direct SHW are 7.9 MWh, 1.8 MWh and 0.4 MWh when collector area is 6 m^2; 7.0 MWh, 1.9 MWh and 1.1 MWh when collector area is 12 m^2; and 6.4MWh, 1.9 MWh and 1.6 MWh when collector area is 18 m^2. The results are also summarised in Table 7. As collector area decreases from 18 m^2 to 6 m^2, the heat provision by

ASHP increases by 23.7% and that by SHW decreases by 46%. At the same time, the heat provision form SWHP slightly decreases by 5.3%. During the non-heating periods, using a collector area of 6 m^2 requires SWHP, even ASHP, for HW while a collector area of 12 m^2 seems sufficient to ensure direct SHW to provide the majority of heat provision.

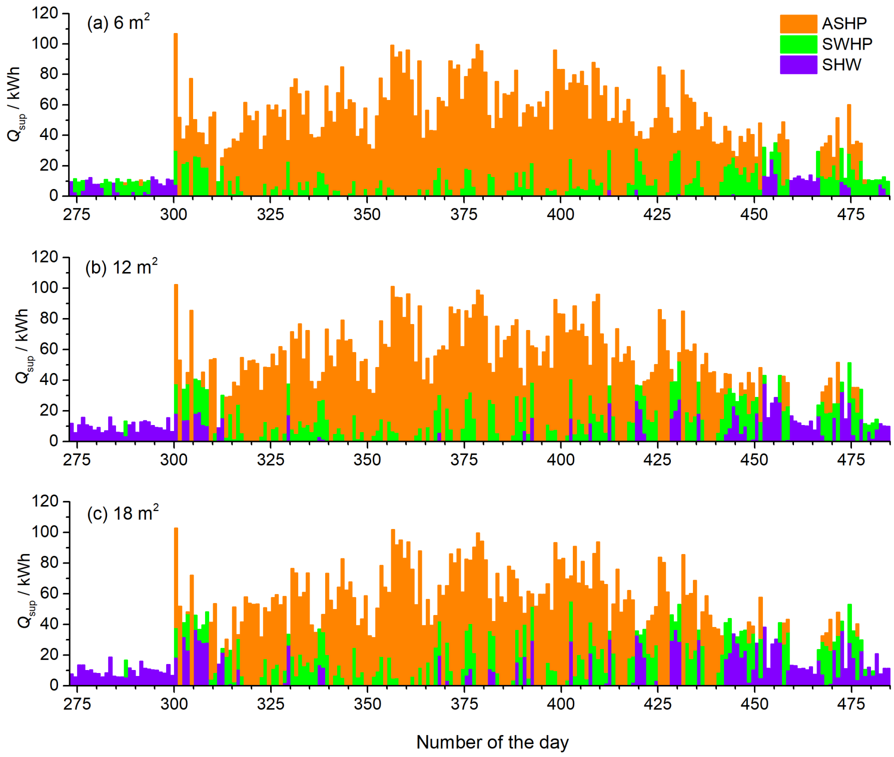

Figure 11: Daily variations of heat provision of the heating system using CPC-CSC for SH and HW by direct SHW, ASHP and SWHP over a heating season

Figure 12 shows the variations of electricity consumption by ASHP, SWHP and pumps. The columns are stacked to represent the total daily electricity consumption. The electricity consumed by ASHP, SWHP and pumps are 2.08 MWh, 0.37 MWh and 0.30 MWh when collector area is 6 m^2; 1.84 MWh, 0.37 MWh and 0.29 MWh when collector area is 12 m^2; and 1.69 MWh, 0.37 MWh and 0.28 MWh when collector area is 18 m^2. The results are also summarised in Table 7. It can be seen that the collector area has mere influence of electricity consumption by SWHP. In terms of ASHP and pumps, decrease in collector area brings more electricity consumption. As collector area decreases, though heat provision from direct SHW decreases, pumps need more frequent for solar collection and thus consumes more electricity.

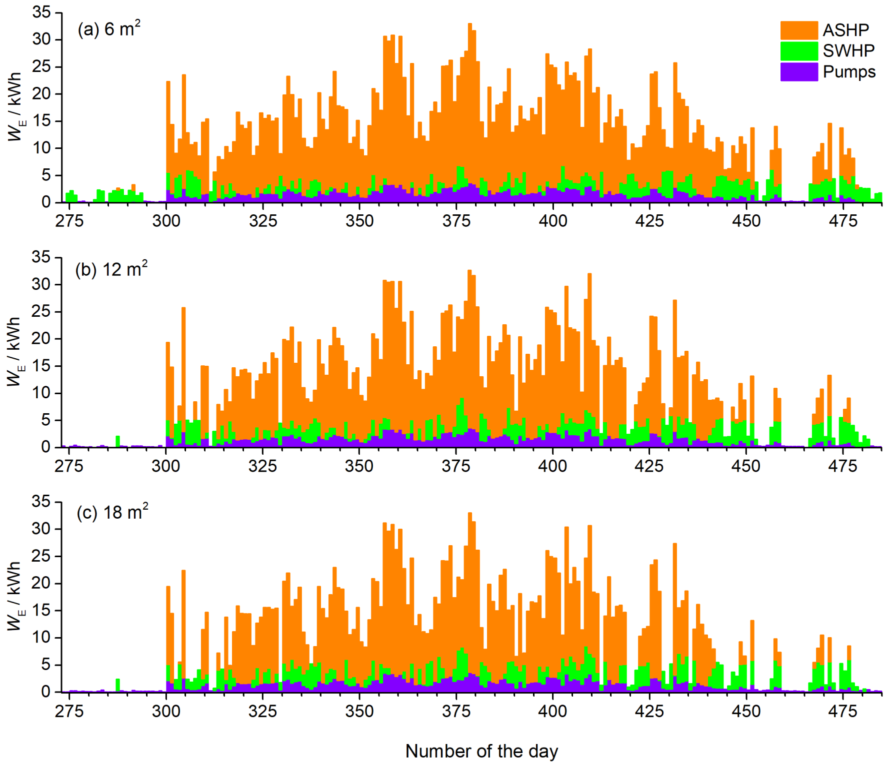

Figure 12: Daily variations of electricity consumption by ASHP, SWHP and pumps of the heating system using CPC-CSC over a heating season

Figure 13 shows the variations of Q_{TES} charged (positive) and discharged (negative) of TES tank 2 over a heating season. Smaller collector area leads to less solar energy collection and thus less thermal energy stored in TES tank 1. Therefore, the capacity of Q_{TES} charged in and discharged from TES tank 2 decreases relatively as collector area decreases.

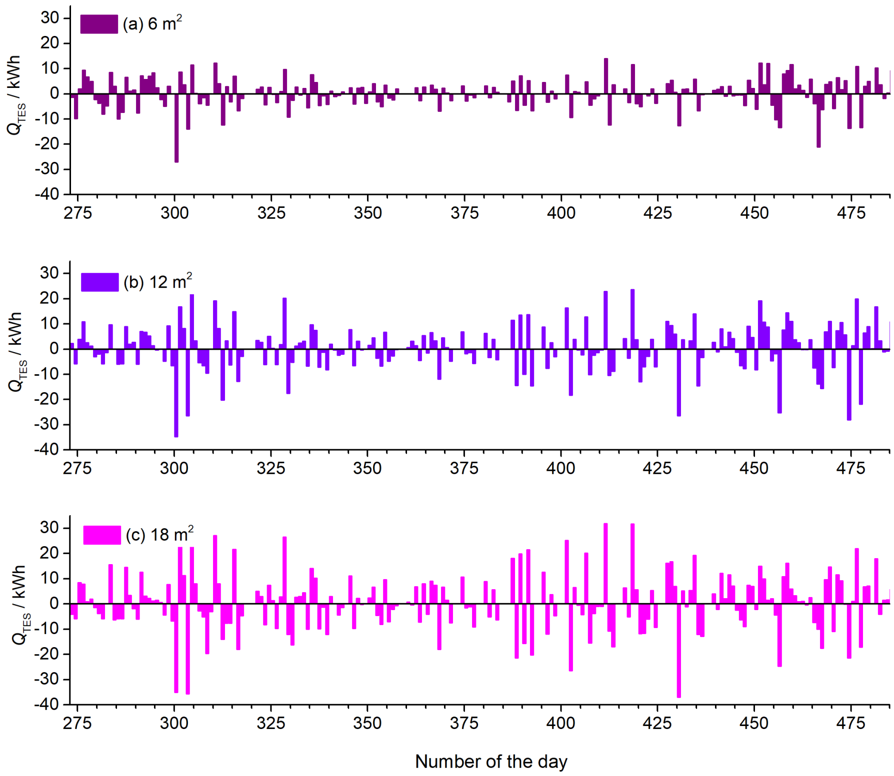

Figure 13: Daily variations of Q_{TES} charged (positive) and discharged (negative) of the heating system using CPC-CSC over a heating season

Figure 14 shows the variations of daily COP_{ASHP} and COP_{SWHP} over a heating season. The average daily COP_{ASHP} is 3.5 for different collector areas while the average daily COP_{SWHP} is 4.8, 5.0 and 5.1 for collector area of 6 m^2, 12 m^2 and 18 m^2. In most time, the COP_{ASHP} is almost the same for different collector areas; in late heating periods, the COP_{ASHP} increases as collector area decreases. This is because that for larger collector area, water temperature in TES tank 1 is higher and ASHP only needs to work at higher ambient temperature while the condensing temperature is also higher, limiting the efficiency of ASHP, especially in late heating periods. COP_{SWHP} generally increases as collector area increases due to large increase in the temperature of heat source. For a system using CPC-CSC of 6 m^2, both ASHP and SWHP are more frequently used, even in non-heating periods.

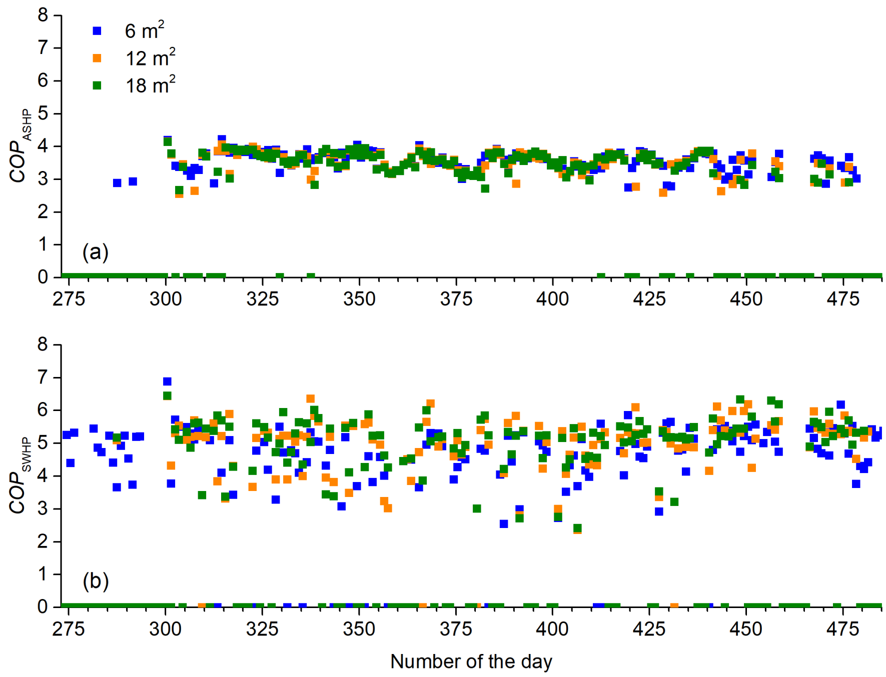

Figure 14: Daily variations of averaged COP_{ASHP} and COP_{SWHP} of the heating system using CPC-CSC over a heating season

Figure 15 shows the variation of *SPF* of heating system using CPC-CSC of different areas over a heating season. The SPF_{ASHP} is 3.8 for different collector areas while the SPF_{SWHP} is 4.9, 5.2 and 5.2 for collector area of 6, 12 and 18 m^2. The seasonal SPF_{sys} is 3.6, 3.9 and 4.2 for collector area of 6, 12 and 18 m^2. It can be seen that in most time, the SPF_{sys} for the system using different collector areas are generally the same. In late heating period (since the 412$^{\mathrm{th}}$ day), the SPF_{sys} shows apparent difference that the system with CPC-CSC of larger area has a larger SPF_{sys}. This is because that as solar availability increases, for larger collector area, more heating is provided by direct SHW and SWHP and the efficiency of SWHP increases as well.

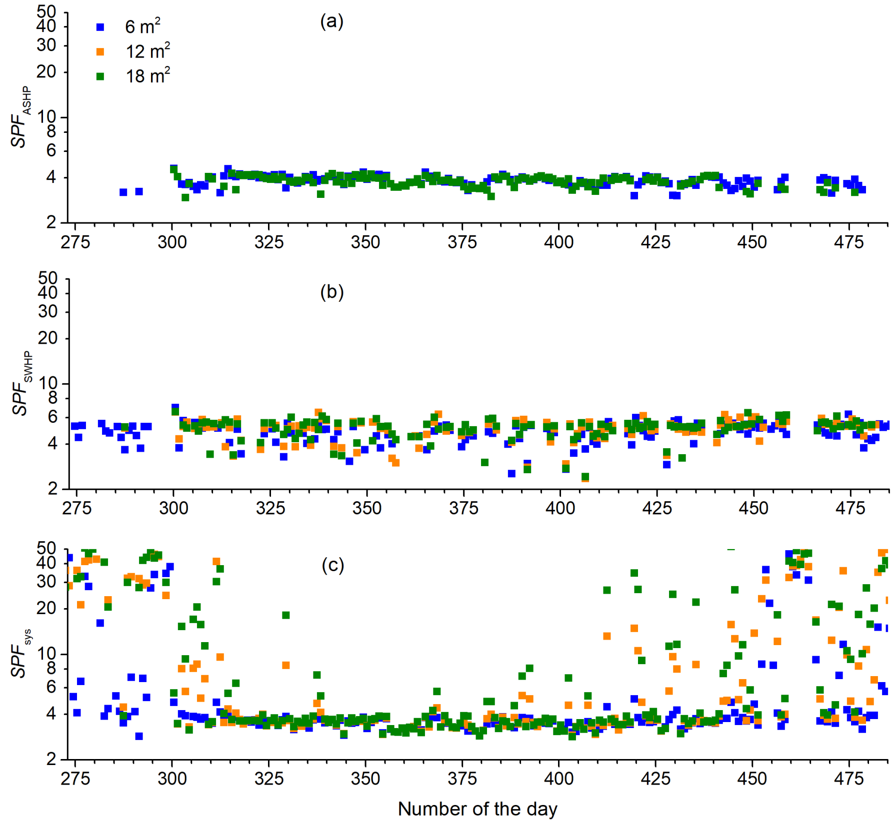

Figure 15: Daily variations of SPF_{ASHP}, SPF_{SWHP} and SPF_{sys} of the heating system using CPC-CSC over a heating season

4.3 Effect of solar collector area on yearly operation performance of heating system

The effect of collector area on the yearly operation performance of the heating system is analysed for collector areas of 6, 9, 12, 15 and 18 m^2. Figure 16 shows the variation of yearly heat provision by ASHP, SWHP and SHW of the heating system using CPC-CSC. As collector area decreases, the heat provision by SWHP is merely changed while that by ASHP increases and that by SHW decreases. As collector area decreases from 18 m^2 to 6 m^2, the heat provision by ASHP is increased by 23.7% and that by SHW is decreased by 46.0%.

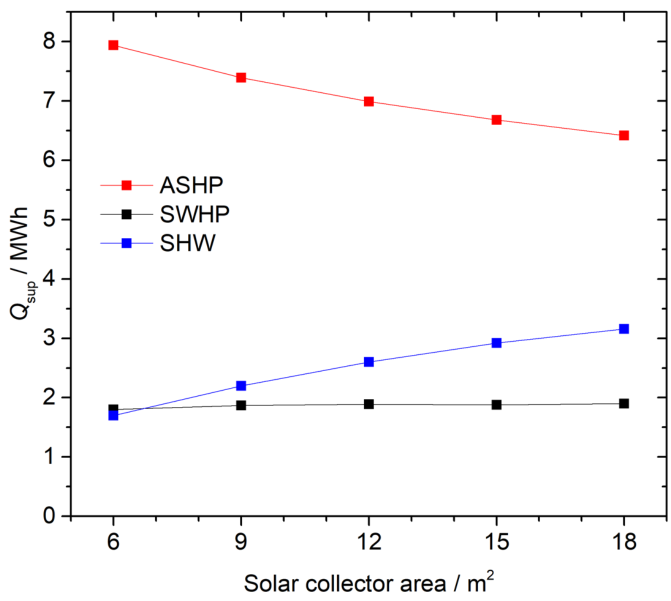

Figure 16: Variations of heat provision for SH and HW by ASHP, SWHP and direct SHW of the heating system using CPC-CSC over a year.

Figure 17 shows the variations of electricity consumption by ASHP, SWHP and pumps. As collector area decreases from 18 m^2 to 6 m^2, electricity consumed by ASHP is apparently increased, by 23.0 %. Electricity consumption by pumps is slightly increased, by 8.1% because pumps need to work more frequently to compensate the low collection capacity of small solar collector. Electricity consumed by SWHP is merely changed.

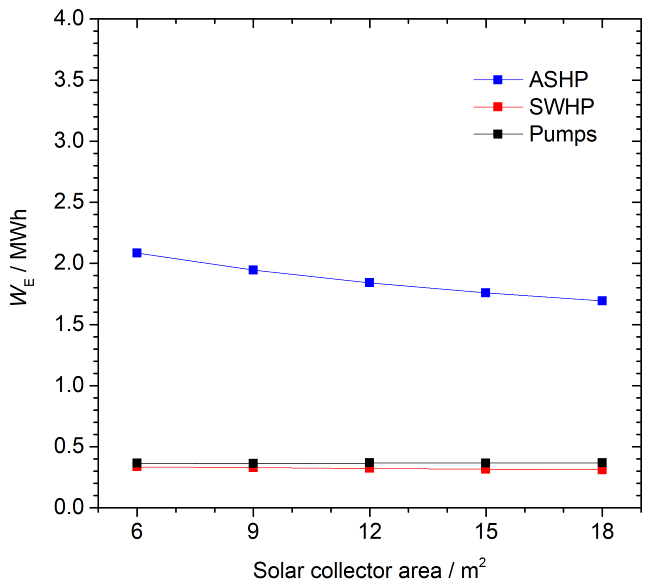

Figure 17: Variations of electricity consumption by ASHP, SWHP and pumps of the heating system using CPC-CSC over a year

Figure 18 shows the variations of thermal energy collected from solar energy and ambient air. As collector area decreases from 18 m^2 to 6 m^2, thermal energy obtained from air is increased by 23.9%. At the same time, thermal energy obtained from solar energy is decreased by 33.8%. The total thermal energy obtained from clean energy is reduced by 5.8%. Both curves change quickly at low collector areas and then slowly at high collector areas. This suggests that the influence of collector area on system performance tends to be insignificant at large collector areas.

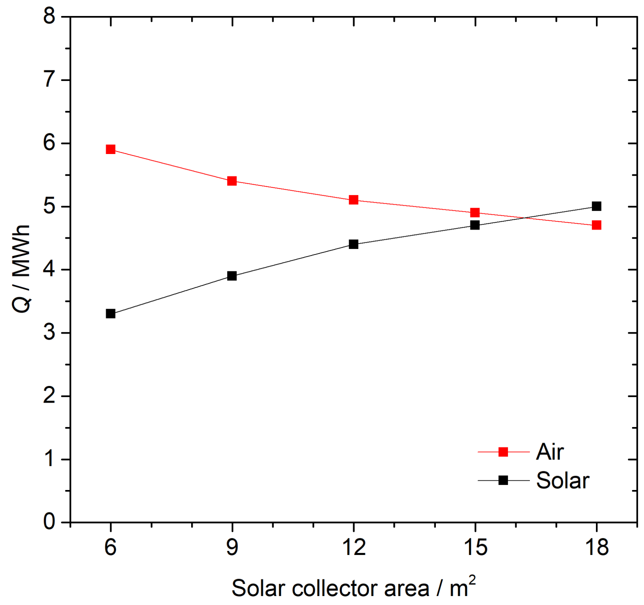

Figure 18: Variation of thermal energy (Q) extracted from solar energy and ambient air of the heating system using CPC-CSC over a year

Figure 19 shows the variations of solar fraction over a year and that over a heating season. With the decrease of collector area from 18 m^2 to 6 m^2, seasonal *SF* decreases from 32.7% to 18.9%; yearly *SF* decreases from 42% to 28.1%. The decrease of *SF* is more significant as collector area decreases from 9 m^2 to 6 m^2, from 23.5% to 18.9% and 33.3% to 28.1% for seasonal and yearly *SF*, respectively.

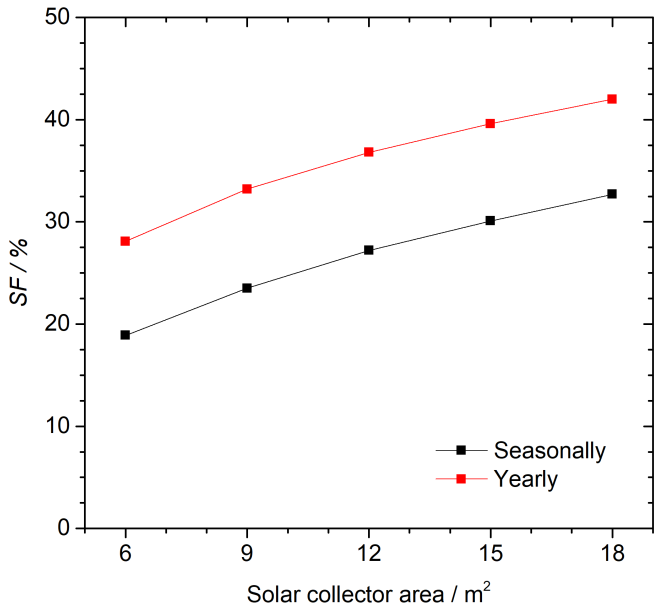

Figure 19: Variations of yearly and seasonally *SF* of the heating system using CPC-CSC

Figure 20 shows the variation of yearly averaged COP_{ASHP} and COP_{SWHP} of the heating system using CPC-CSC. The COP_{ASHP} is almost the same for different collector areas, at around 3.5. COP_{SWHP} is generally around 5.0 but shows a slight decreasing trend as collector area decreases. Especially, as collector area decreases from 9 m^2 to 6 m^2, COP_{SWHP} is decreased by 4.0% while as collector area decreases from 18 m^2 to 6 m^2, COP_{SWHP} is decreased by 5.9%.

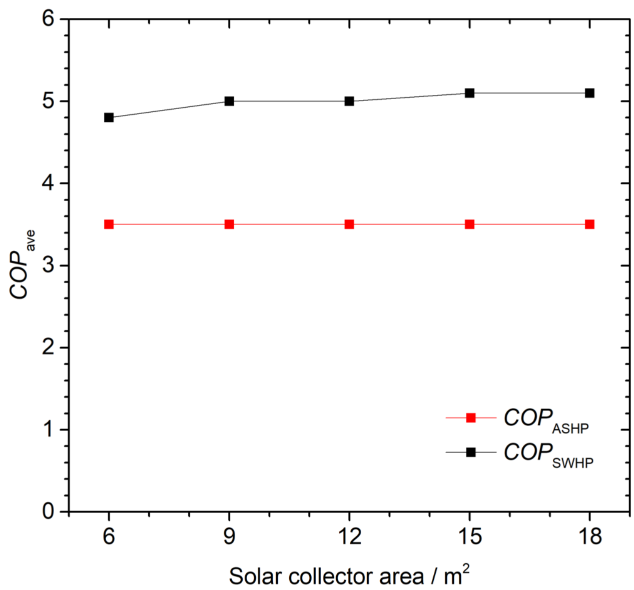

Figure 20: Variations of averaged COP_{ASHP} and COP_{SWHP} with solar collector area of the heating system using CPC-CSC over a year

Figure 21 shows the variations of *SPF* of the heating system using CPC-CSC. SPF_{ASHP} remains consistent for different collector areas, at around 3.8. SPF_{SWHP} keeps even at collector area no smaller than 9 m^2, at around 5.2. As collector area decreases from 9 m^2 to 6 m^2, SPF_{SWHP} decreases by 5.8%. As collector area decreases from 18 m^2 to 6 m^2, seasonal and yearly SPF_{sys} decrease by 14.3% and 14.9%. Compared with the system in Table 1, this heating system using CPC-CSC achieves acceptable system efficiency, even at lower collector area.

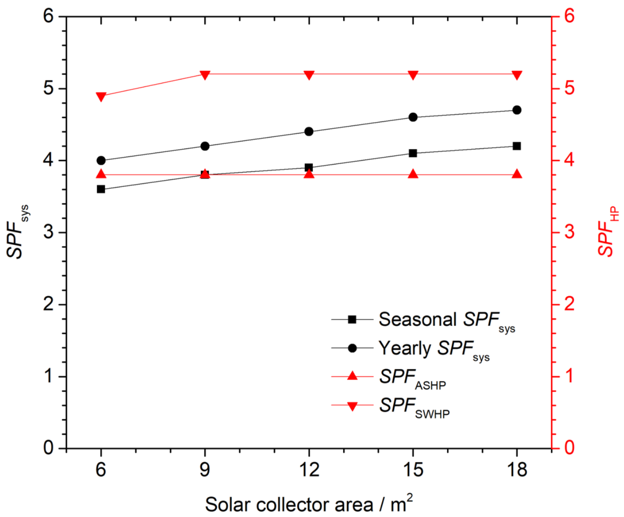

Figure 21: Variations of yearly and seasonally SPF_{HP} and SPF_{sys} of the heating system using CPC-CSC.

Details for the operation performance of the SAASHP using CPC-CSC of different areas are listed in table 8. For comparison, performance of SAASHP using FPC of 18 m^2 are also included. It can be seen that, at the same collector area, the yearly solar energy used by the system using CPC-CSC is 306.8 kWh higher than that of system using FPC. For almost same SPF_{sys}, the area of the CPC-CSC required is 12 m^2 while the area required for the FPC is 18 m^2, reduced by one third. This benefits to reduce the scale of SAASHP and promote its popularity.

Table 8: Operation performance of the IX-SAASHP heating system integrating CPC-CSC

System		Period	Using CPC-CSC					Using FPC
			6	9	12	15	18	18
Heat provision (kWh)	HW	Heating season	2238.7	2238.1	2238.0	2237.9	2237.9	2237.7
		Non-heating season	1427.6	1427.5	1427.3	1427.2	1427.2	1427.5
	SH		7523.9	7522.9	7524.5	7521.6	7520.3	7527.9
	Total		11190.1	11188.5	11189.8	11186.7	11185.4	11193.1
Heat provision (kWh)	SWHP		1802.8	1874.3	1886.7	1881.5	1903.8	2289.1
	ASHP		7942.8	7393.4	6990.3	6679.9	6419.6	6586.6
	Solar	Heating season	403.9	781.9	1134.2	1423.2	1649.7	1187.6
		Non-heating season	1299.2	1415.2	1464.9	1494.8	1511.1	1409.4
Electricity consumption (kWh)	SWHP		365.1	362.4	365.5	364.7	366.2	449.2
	ASHP		2083.5	1944.6	1841.3	1757.8	1692.3	1737.7
	Water pumps	Heating season	300.8	293.0	286.7	280.3	275.7	295.0
		Non-heating season	34.1	35.8	35.5	34.3	34.0	40.7
	Total		2783.4	2635.8	2529.0	2437.0	2368.1	2522.6
$\boldsymbol{SPF}_{\mathrm{HP}}$	SWHP		4.9	5.2	5.2	5.2	5.2	5.1
	ASHP		3.8	3.8	3.8	3.8	3.8	3.8
$\boldsymbol{COP}_{\mathrm{ave}}$	SWHP		4.8	5.0	5.0	5.1	5.1	5.0
	ASHP		3.5	3.5	3.5	3.5	3.5	3.5
Solar thermal energy (kWh)	To SWHP		1437.7	1512.0	1521.1	1516.9	1537.6	1839.9
	To end use	Heating season	403.9	781.9	1134.2	1423.2	1649.7	1187.6
		Non-heating season	1299.2	1415.2	1464.9	1494.8	1511.1	1409.4
	Total		3317.8	3939.4	4376.8	4719.4	5013.5	4706.7
Thermal energy from ambient air (kWh)			5859.3	5448.8	5149.0	4922.1	4727.3	4848.9
$\boldsymbol{SF}$	Heating season		18.9%	23.5%	27.2%	30.1%	32.7%	31.0%
	Yearly		28.1%	33.2%	36.8%	39.6%	42.0%	39.6%
$\boldsymbol{SPF}_{\mathrm{sys}}$	Heating season		3.6	3.8	3.9	4.1	4.2	3.9
	Yearly		4.0	4.2	4.4	4.6	4.7	4.4

5. Economic Analyses

Economic analysis for SAASHP heating system using CPC-CSC of different areas are conducted according to the electricity price in UK. W_{tot} is the total electricity consumption of the heating systems, given by Eq. (24):

$$W_{tot} = (Q_{SH} + Q_{HW} - Q_{re})/\eta \tag{24}$$

where η is the efficiencies of electric heater and gas boiler, Q_{re} is the renewable energy used by the system.

P_{pb} is the payback period of the heating systems against electric heater, calculated by Eq. (25):

$$P_{pb} = C_i / C_{spy} \tag{25}$$

where C_i is the difference of the initial cost and C_{spy} is the cost saving per year, obtained by Eqs. (26) and (27).

$$C_i = C_{i0} - C_{ieh} \tag{26}$$

$$C_{spy} = C_{o0} - C_{oeh} \tag{27}$$

where C_{i0} and C_{ieh} are the initial costs of the heating system and the electric heater, C_{o0} and C_{oeh} are the operation costs of the heating system and the electric heater.

The efficiencies of the electric heater and gas boiler are obtained from [33], 0.95 and 0.85. The heat provision of electric heater and gas boiler is set to be the average heat provision of the SAASHP heating system. The electricity and gas prices are obtained from E.On Energy (a UK energy suppler) to be £400.2 per MWh and £106.8 per MWh (prices in June 2022) [34]. Currently, the price of CPC collector is around twice of that of ETC [24]. Since CPC-CSC is a new collector in research and development status, price of ETC is adopted to assume CPC-CSC price after commercialisation. The prices of electric heater and gas boiler of 8 kW [35], TES tank of 300 L and 500 L [36], water pump with a heat of 10 m [37], flat plate collector [38] and evacuated tube collector [39] are obtained from UK domestic and European sellers. The price of heat pump is assumed based on UK government report [40]. Installation for SHW system is assumed to be 3 hours and that for SAASHP is assumed to be 6 hours. The engineer fee is taken to be £80 per hour [41]. The economic analysis for SAASHP heating system integrating CPC-CSC of different areas is displayed in table 9 according to energy prices in 2022.

Table 9: Economic analysis for electric heater, direct SHW and SAASHP heating systems based on the energy prices in June, 2022

		Electric water heater	**Gas boiler**	**Electric heater boosted SHW**	**Gas boiler boosted SHW**	**SAASHP (FPC)**	**SAASHP (CPC-CSC)**				
Collector area		-	-	18	18	18	6	9	12	15	18
Heat provision per year, MWh		11.19	11.19	11.19	11.19	11.19	11.19	11.19	11.19	11.19	11.19
Efficiency/performance		0.95	0.85	0.95	0.85	*SPF*=4.4	*SPF*=4.0	*SPF*=4.2	*SPF*=4.4	*SPF*=4.6	*SPF*=4.7
Energy consumption per year, MWh		11.8	13.2	7.2	8.0	2.2	2.5	2.4	2.2	2.1	2.1
Initial cost, £	collector	0	0	4230	4230	4230	1620	2430	3240	4050	4860
	tanks	765	765	2195	2195	2195	2195	2195	2195	2195	2195
	Heater/HP	890	890	890	890	6000	6000	6000	6000	6000	6000
	pumps	0	0	220	220	330	330	330	330	330	330
	Installation	0	0	240	240	480	480	480	480	480	480
	total	1655	1655	7775	7775	13235	10625	11436	12245	13055	13865
Operation cost, £		4714.3	1406.5	2881.7	854.7	897.8	999.6	946.3	897.8	853.5	832.8
Cost saving per year, £		-	3307.8	1832.6	3859.6	3816.5	3714.7	3768.0	3816.5	3860.8	3881.5
Payback period, year		-	-	3.34	1.57	3.03	2.41	2.60	2.77	2.95	3.15

It can be seen that, though the unit price of FPC is assumed to be 25% cheaper than that of CPC-CSC, at current electricity price, the SAASHP heating system using CPC-CSC can have an 8.6% shorter payback period to the SAASHP heating system using FPC of the same SPF_{sys}. For CPC-CSC of different areas, SPF_{sys} and the payback period decrease as collector area decrease. As collector area decreases from 18 m^2 to 6 m^2, payback period decreases by 23.5%. According to both system performance and economic analyses, for domestic heating of an SFH 45 building in London, it is potential to reduce the required size of CPC-CSC to 9 m^2 and even less. Since solar collector with a smaller size can much easily be adopted for domestic use, using CPC-CSC benefits to wide rollout of SAASHP heating systems for domestic heating.

6. Conclusions

In this work, the solar assisted air source heat pump heating system integrating compound parabolic concentrator-capillary tube solar collector has been modelled and numerically simulated. The operation performance of this heating system are compared with that of the heating system using flat plate collector. The effect of the solar collector size on the operation performance and economics of the heating sytem have been analysed. The following conclusions can be drawn:

1. For same SPF_{sys}, the size of the CPC-CSC required is 12 m^2 whereas the size of the FPC required is 18 m^2, leading to one third reduction in solar collector size.
2. Compared with system using FPC, the heat provision from SWHP is significantly reduced by 17.4% using CPC-CSC and the heat provision by ASHP is slightly reduced by 3.0%. heat provision by direct SHW is apparently increased by 41.7%.
3. For the heating systems using same size solar collector of 18 m^2, the CPC-CSC reduces the electricity consumption by 154.5 kWh per year (123.6 kg CO_2 equivalent) compared with the FPC. Increase in the utilisation of solar energy is 306.8 kWh. Hence, the seasonal performance factor is increased from 4.4 to 4.7.
4. As collector size decreases, both SPF_{sys} and the payback period decreases. As collector area decreases from 18 m^2 to 6 m^2, seasonal and yearly SPF_{sys} decrease by 14.3% and 14.9% while payback period decreases by 23.5%. Considering both thermal and economic performances, the size of the concentrated solar collector could potentially be reduced to 9 m^2 or less.
5. As collector area decreases from 18 m^2 to 6 m^2, the heat provision by ASHP increases by 23.7% and that by SHW decreases by 46%, the electricity consumed by ASHP and the

pumps increase by 23 % and 8.1%. For SWHP, the heat provision slightly decreases by 5.3% and the electricity consumption is merely influenced.

Acknowledgements

The authors gratefully acknowledge the financial supports from the Joint PhD Studentship of China Scholarship Council (CSC) and Queen Mary University of London (201808060459), National Natural Science Foundation of China (51506004) and the Wuhan Applied Foundational Frontier Project (No. 2020010601012172).

Nomenclature

A	collector area, m^2
C_{i}	initial cost difference, GBP
C_{i0}	initial cost of the studied system, GBP
C_{ieh}	initial cost of the electrical water heater, GBP
C_{o0}	operation cost of the studied system, GBP
C_{oeh}	operation cost of the electrical water heater, GBP
COP	coefficient of performance
CR	concentration ratio
C_{spy}	cost saving per year, GBP
c	specific heat of working fluid, J/kg-K
D	aperture width, mm
d	outer diameter of the capillary tube absorber, mm
HC	heating capacity, kW
P_{pb}	payback period, year
$Q_{\mathrm{ASHP,\ con}}$	heat transferred from the condenser of ASHP, kWh
$Q_{\mathrm{HP,\ con}}$	thermal energy obtained at the condenser of a heat pump, kWh
Q_{HW}	thermal energy for hot water, kWh
$Q_{\mathrm{loss,\ SC}}$	heat loss from solar collector, kWh
Q_{loss}	heat loss from the CPC-CSC per meter (along length), kWh
Q_{re}	renewable energy used in the system, kWh
Q_{SC}	thermal energy obtained by solar collector, kWh
Q_{SH}	thermal energy for space heating, kWh

$Q_{\mathrm{SWHP,\ con}}$	heat transferred from the condenser of SWHP, kWh
Q_{su}	solar energy used, kWh
Q_{sup}	thermal energy supply, kWh
Q_{TES}	thermal energy storage, kWh
I	solar irradiance on tilted surface, $\mathrm{W/m^2}$
m	mass flow rate, kg/s
SF	solar fraction
SPF_{HP}	seasonal performance factor of the heat pump
SPF_{sys}	seasonal performance factor of the system
T_{amb}	ambient air temperature, $^{\circ}\mathrm{C}$
T_{indoor}	indoor temperature, $^{\circ}\mathrm{C}$
T_{in}	temperature of working fluid at inlet of CPC-CSC, $^{\circ}\mathrm{C}$
T_{out}	temperature of working fluid at outlet of CPC-CSC, $^{\circ}\mathrm{C}$
T_{SC}	temperature of solar collector, $^{\circ}\mathrm{C}$
T_{HWS}	outlet temperature of hot water tank, $^{\circ}\mathrm{C}$
v_{a}	wind speed, m/s
W_{ASHP}	electricity consumed by air source heat pump, kWh
W_{HP}	electricity consumed by a heat pump, kWh
W_{pumps}	electricity consumed by pumps, kWh
W_{SWHP}	electricity consumed by solar water heat pump, kWh
W_{tot}	total electricity consumed, kWh

Greek Letter

η	efficiency of electric heater and gas boiler systems
φ	angle between the incidence and the X axis
θ_{A}	aperture angle of the CPC

Abbreviation

ASHP	air source heat pump
CPC	compound parabolic concentrator
CSC	capillary-tube solar collector

ETC	evacuated-tube collector
FPC	flat plate collector
HC	heating capacity
HW	hot water
SAASHP	solar-assisted air source heat pump
SC	space cooling
SFH	single family house
SH	space heating
SHW	solar hot water
SWHP	heat pump that uses hot water from solar collector as heat source
TES	thermal energy storage
TRNSYS	TRaNsient SYstem Simulation program

References

[1] Yang LW, Xu RJ, Hua N, Xia Y, Zhou WB, Yang T, Belyayev Ye, Wang HS, Review of the advances in solar-assisted air source heat pumps for the domestic sector, Energy Convers Manage 2021; 247: 114710.

[2] Ruschenburg J, Herkel S, Henning HM, A statistical analysis on market-available solar thermal heat pump systems, Solar Energy, 95 (2013) 79–89

[3] Liang CH, Zhang XS, Li XW, Zhu X, Study on the performance of a solar assisted air source heat pump system for building heating, Energy and Buildings, 43 (2011) 2188–2196

[4] Huan C, Wang FH, Li ST, Zhao YJ, Liu L, Wang ZH, Ji CF. A performance comparison of serial and parallel solar‐assisted heat pump heating systems in Xi'an, China. Energy Sci Eng 2019;7:1379-1393.

[5] Vega J, Cuevas C. Parallel vs series configurations in combined solar and heat pump systems: a control system analysis. Appl Therm Eng 2020;166:114650.

[6] Liu ZJ, Liu YW, Wu D, Jin GY, Yu HC, Ma WS. Performance and feasibility study of solar-air source pump systems for low-energy residential buildings in Alpine regions. Journal of Cleaner Production 2020;256:120735.

[7] Caglar A, Yamalı C. Performance analysis of a solar-assisted heat pump with an evacuated tubular collector for domestic heating. Energy Buildings 2012;54:22–28.

[8] Wang Q, Ren B, Zeng ZY, He W, Liu YQ, Xu XG, Chen GM. Development of a novel indirect-expansion solar-assisted multifunctional heat pump with four heat exchangers. Building Services Eng Res Tech 2015;36:469–481.

[9] Shan M, Yu T, Yang X. Assessment of an integrated active solar and air-source heat pump water heating system operated within a passive house in a cold climate zone. Renew Energy 2016;87:1059-1066.

[10] Kuang YH, Wang RZ, Yu LQ, Experimental study on solar assisted heat pump system for heat supply, Energy Conversion and Management 44 (2003) 1089–1098

[11] He W, Hong XQ, Zhao XD, Zhang XX, Shen JC, Ji J, Operational performance of a novel heat pump assisted solar façade loop-heat-pipe water heating system, Applied Energy, 146 (2015) 371–382

[12] Buker SM, Riffat SB. Build-up and performance test of a novel solar thermal roof for heat pump operation. Int J Ambient Energy 2017;38:365-379.

[13] Lee SJ, Shon BH, Jung CW, Kang YT. A novel type solar assisted heat pump using a low GWP refrigerant (R1233zd(E)) with the flexible solar collector. Energy 2018;149:386-396.

[14] Kim T, Choi BI, Han YS, Do KH. A comparative investigation of solar-assisted heat pumps with solar thermal collectors for a hot water supply system. Energy Convers Manage 2018;172:472-484.

[15] Treichel C, Cruickshank CA. Energy analysis of heat pump water heaters coupled with air-based solar thermal collectors in Canada and the United States. Energy 2021;221:119801.

[16] Treichel C, Cruickshank CA. Greenhouse gas emissions analysis of heat pump water heaters coupled with air-based solar thermal collectors in Canada and the United States. Energy Buildings 2021;231:110594.

[17] Gao C, Chen F, Model building and optical performance analysis on a novel designed compound parabolic concentrator, Energy Conversion and Management 209 (2020) 112619

[18] Chen XM, Yang XD, Solar collector with asymmetric compound parabolic concentrator for winter energy harvesting and summer overheating reduction: Concept and prototype device, Renewable Energy 173 (2021) 92-104

[19] Zheng WD, Yang L, Zhang H, et al. Numerical and experimental investigation on a new type of compound parabolic concentrator solar collector. Energy Convers Manage 2016;129:11–22.

[20] Chamsa-Ard W, Sukchai S, Sonsaree S, et al. Thermal performance testing of heat pipe evacuated tube with compound parabolic concentrating solar collector by ISO 9806–1. Energy Procedia 2014;56:237–46.

[21] Wang Y, Zhu Y, Chen H, et al. Performance analysis of a novel sun-tracking CPC heat pipe evacuated tubular collector. Appl Therm Eng 2015;87:381–8.

[22] Xu RJ, Zhao YQ, Chen H, Wu Q, Yang LW, Wang HS. Numerical and experimental investigation of a compound parabolic concentrator-capillary tube solar collector. Energy Convers Manage 2020;204:112218.

[23] Indira SS, Vaithilingam CA, Sivasubramanian R, Chong KK, Saidur R, Narasingamurthi K, Optical performance of a hybrid compound parabolic concentrator and parabolic trough

concentrator system for dual concentration, Sustainable Energy Technologies and Assessments 47(2021)101538
[24] Wei B, Wang YZ, Liu ZJ, Liu BX, Optimization study on a solar-assisted air source heat pump system with energy storage based on the economics method. Int J Energy Res 2020;44:2023–2036.
[25] Chen YZ, Li XX, Hua HL, Lund PD, Wang J, Exergo-environmental cost optimization of a solar-based cooling and heating system considering equivalent emissions of life-cycle chain, Energy Conversion and Management 258(2022) 115534
[26] Dott R, Haller MY, Ruschenburg J, Ochs F, Bony J, The Reference Framework for System Simulations of the IEA SHC Task 44 / HPP Annex 38—Part B: Buildings and Space Heat Load, A technical report of subtask C—Report C1 Part B, International Energy Agency, 2013.
[27] Yang LW, Hua N, Pu JH, Xia Y, Zhou WB, Xu RJ, Yang T, Belyayev Ye, Wang HS, Analysis of operation performance of three indirect expansion solar assisted air source heat pumps for domestic heating, Energy Convers Manage 2022; 252: 115061.
[28] Zhang D, Tao H, Wang M, et al. Numerical simulation investigation on thermal performance of heat pipe flat-plate solar collector. Appl Therm Eng 2017;118:1
[29] GB/T 4271-2007 Test methods for the thermal performance of solar collectors [Chinese], http://www.csres.com/detail/184924.html [accessed on August 9th, 2022]
[30] Dickes R, Lemort V, Quoilin S, Semi-empirical correlation to model heat losses along solar parabolic trough collectors Proceedings of ECOS 2015-28th International Conference on Efficiency, Cost, Optimization, Simulation and Environmental Impact of Energy Systems. Pau, France: ECOS, 2015.
[31] World Health Organization, LEGIONELLA and the prevention of legionellosis, 2007.
[32] Charted Institute of Plumbing and Heating Engineering, https://www.ciphe.org.uk/consumer/safe-water-campaign/hot-water-scalds/, [accessed on June 8th, 2022].
[33] Li H, Yang HX, Potential application of solar thermal systems for hot water production in Hong Kong, Appl Energy 2009; 86: 175–180.
[34] E.ON Energy, https://www.eonenergy.com/for-your-home/products-and-services/best-deal-for-you/quote, [accessed on June 8th, 2022].
[35] https://www.screwfix.com/c/heating-plumbing/boilers/cat6660001?boilertype=combi#category=cat6660001&boilertype=heat_only [accessed on October 8th, 2022]
[36] https://www.screwfix.com/p/rm-cylinders-500ltr-indirect-unvented-hot-water-storage-cylinder/8141p [accessed on October 8th, 2022]
[37] https://www.machinemart.co.uk/categories/?search=Electric+Pump&Category=Water+Pumps&Max%20Head=14+m [accessed on October 8th, 2022]

[38] https://www.heiz24.de/Flat-plate-collector-Sunex-type-AMP-251-250qm-New?curr=EUR&gclid=EAIaIQobChMIicej1bzR-gIVpWLmCh3Q0wEEEAQYASABEgKuzfD_BwE [accessed on October 8th, 2022]
[39] https://www.bimblesolar.com/solar-thermal-30-tube [accessed on October 8th, 2022]
[40] Committee on Climate Change, The Sixth Carbon Budget -- The UK's path to Net Zero, 2020, https://www.theccc.org.uk/publication/sixth-carbon-budget/
[41] Plumber Costs: 2021 Call Out Charges & Hourly Prices UK, https://tradesmencosts.co.uk/plumbers/ [accessed on June 8th, 2022]